International Journal of Modern Manufacturing Technologies
ISSN 2067–3604, Vol. XVI, No. 1 / 2024
https://doi.org/ 10.54684/ijmmt.2024.16.1.51

MULTI-OBJECTIVE OPTIMIZATION OF ROTARY ASSISTED ELECTROCHEMICAL ARC DRILLING (R-ECAD) PROCESS USING GRA

Sahil Grover, Viveksheel Rajput, Sanjay Kumar Mangal, Sarbjit Singh, Sanjeev Kumar

Mechanical Engineering Department, Punjab Engineering College, Sector 12, Chandigarh, 160012, India

Corresponding author: Viveksheel Rajput, sheelrajput03@gmail.com

Abstract: Electrochemical Arc Drilling (ECAD) has demonstrated its effectiveness in micro-machining a variety of materials notwithstanding the inherent properties of materials. The increased machining properties of the ECAD method are a result of the inclusion of rotational effect of the working material. Better electrolyte replenishment, effective debris flushing, thin gas layer development, and spark uniformity are all credited with this improvement. Several input factors affect the machining characteristics of ECAD, making it difficult to simultaneously optimize these factors for several objectives. In order to maximise Material Removal Rate (MRR) and minimising Hole Overcut (HOC), this paper focuses on the multi-objective optimization of rotary-assisted ECAD (R-ECAD) input factors. Taguchi's L9 experimental design is used to produce micro-holes, and then Grey Relational Analysis (GRA) is used to perform the multi-objective optimization. The chosen input factors are working material rotation (WR), tool feed rate (FR) and applied voltage (V), whereas the chosen response factors are MRR and HOC. Results indicate that the rotating effect of the working material, which aids in the replenishment of electrolyte and the creation of a stable gas layer surrounding the tool, is notably the most significant input factor. For maximising the MRR and minimising HOC, the GRA-based optimised factors were found to be AIICIIBIII (60 rpm, 40 V, 0.8 mm/min). The responses are greatly improved by 39% as compared to the original machining, as demonstrated by microscopy images obtained during the GRA-based input factor optimization.
Key words: Grey relational analysis, overcut, sparks, multi-objective, material removal, optimization.

1. INTRODUCTION

The need for micro-sized components has grown significantly in recent years, owing to their extensive use in a variety of sectors, including food and beverage, medical applications [1] etc. Electrochemical Discharge cutting (ECAD) is the preferred method for cutting non-conductive materials such as glass, ceramics, and silicon. These materials have a variety of favourable features, such as chemical inertness, translucency, high hardness, and outstanding thermal insulation. These characteristics make them ideal for practical applications in micro-reactors, micro-pumps, and micro-reactors. However, creating micro-features on these non-conductive materials provides an intimidating challenge when using unconventional lithography and thermal energy approaches. Due to the production of a significant heat-affected zone, these technologies have limited process capacity, limiting their applicability in a variety of industrial applications [2]. ECAD has evolved as a popular and widely used process for micromachining not only glass but also ceramics, polymer matrix composites, and semiconductor materials, providing a feasible option to overcome the limits of traditional methods. Numerous industries face a substantial barrier in producing advanced 3D microstructures on materials such as glass, ceramics, and silicon. These materials are in great demand for a variety of applications, including micro-biological labs, micro-electro-mechanical systems (MEMS), micro-pumps, micro-reactors, and a variety of other purposes [3-6]. Traditional technologies, like as lithography and thermal energy-based methods, fall short in terms of their ability to effectively create such components. This restriction is principally due to the possibility of surface degradation and the formation of major heat-affected zones [7-10]. When it comes to dealing with non-conductive materials, ECAD has specific benefits over conventional drilling technologies. It excels at producing high-quality surface finishes while maintaining an admirable machining pace. Glass is widely used in a variety of sectors owing to its exceptional resistance to chemical and heat impacts [11]. However, because of its intrinsic brittleness, which causes material to fracture quickly when exposed to conventional machining techniques, machining glass is one of the most difficult undertakings.

The basic ECAD setup, as shown in Figure 1, consists of several key components: a machining chamber or electrolyte container filled with an aqueous electrolyte solution, a tool electrode, a counter electrode with a larger surface area than the tool electrode, the workpiece material, and a DC power supply. The workpiece, tool

electrode, and counter electrode are all immersed in the electrolyte in this configuration. The tool is positioned immediately above the workpiece, with the counter electrode set at a fixed distance from the tool electrode. The tool has a connection to the negative terminal, while the counter electrode is connected to the positive terminal of the DC power source. As the voltage is continuously raised, hydrogen gas bubbles develop around the tool's tip. These bubbles eventually combine to form a gas coating that envelops the tool tip. When the voltage is increased higher, the gas film ruptures, resulting in sparks between the tool and the workpiece. Through processes such as melting, evaporation, and chemical etching, these sparks efficiently remove material from the workpiece. The critical voltage is the voltage level at which this gas film rupture occurs. Figure 1(a), (b), and (c) show the phases of gas film creation as the voltage steadily rises and spark production [12-13].

Researchers have worked relentlessly to improve the ECAD technique, with the goal of making it the go-to technique for high-aspect-ratio micro-structure machining. Their goal has been to attain the highest capacity while maintaining impeccable finish quality. Several important discoveries have resulted from this investigation.

Several researchers have investigated several electrolytes in ECAD and discovered that voltage was the most important factor, with electrolyte content acting as a secondary factor influencing the machining process. They discovered that KOH outperformed H_2SO_4 in machining soda lime glass, with applied voltage emerging as a critical component that positively affected MRR [14-16].

S.F. Huang and team successfully drilled micro-holes in SS-304 using pure water as the electrolyte, and they reduced tool wear by increasing tool rotation, voltage, and tool electrode diameter. Notably, they discovered that tool wear rate had an inverse connection with machining voltage, followed by tool rotation and diameter size [17]. According to B. Jiang's study, using tapered tools eliminated small sparks, maintaining a steady spark. Furthermore, they devised and presented conical tools to solve the problem of non-uniform spark dispersion noticed with cylindrical tools, resulting in a more constant and stronger spark. However, it is crucial to highlight that the use of conical tools prompted concerns regarding tool temperature and possible damage [18,19].

Furthermore, the researchers discovered that decreasing the density and surface tension of the electrolyte could possibly reduce the critical voltage. The rate of bubble and film formation was shown to be directly related to current density, but tool immersion depth and size were found to be inversely proportional to current density [20-24]. Various other researchers demonstrated the use of different tool shapes and other input factors on machining performance of the ECAD process [25-30].

The formation of the gas film is critical to achieving successful and uniform machining. Existing research has shown that the creation of this gas layer is dependent on a number of input variables, including localized heating [31], the wetting properties of the tool electrode [32], current, and voltage.

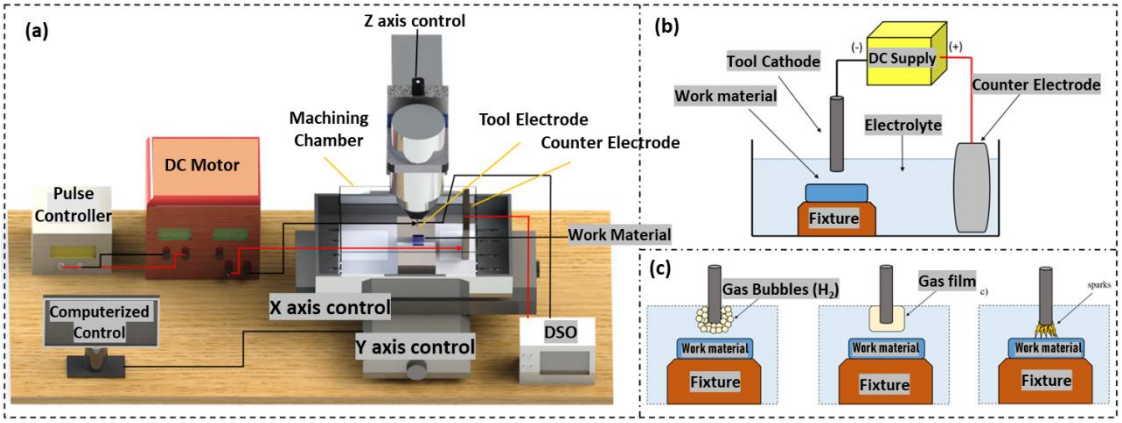

Fig. 1. Schematic representation of ECAD process [25]

Cheng et al. [33] performed a thorough investigation of gas film generation during the microhole machining process in important research. They underlined that the gas film structure changes abruptly in response to fluctuations in current signals and may be used as a guideline for enhancing gas film formation efficiency. Their results clearly imply that localized joule heating is the key mechanism driving gas film development. In ECAD, the heat generated as an outcome of the electrical breakdown inside the gas film is an essential component that influences the material removal process directly or indirectly [34]. The thermal energy emitted by these electrochemical discharges largely determines the process performance of ECAD. It's also worth noting that the nature of these discharges is intrinsically linked to the thickness of the gas film [35]. As a result, in ECAD, the thickness of the gas film plays a critical role in controlling the process mechanism and, as a result, determines overall process performance. To fully realize the ECAD process's potential, various researchers have focused their

efforts to making it the best option for high-aspect-ratio micro-structure machining, with high throughput and great finish quality. Harugade et al. [36] did comprehensive study on several electrolytes in ECAD and discovered that voltage is the major variable, with electrolyte concentration having a secondary function in machining. They discovered that when machining soda lime glass, KOH outperformed H_2SO_4, with applied voltage being the most important factor determining material removal rates (MRR) [36]. P.K. Gupta and colleagues experimented with cutting glass with a stainless-steel tool while varying the working spacing. They discovered that a working gap of zero resulted in the least amount of Central Unremoved Material (CURM) and Hole Overcut (HOC). The MRR became insignificant when the working gap approached 250 microns. Furthermore, they discovered that employing a sharp-edged tool improved the discharge process and increased electrolyte flushing, resulting in lower HOC and CURM [37].

The tool rotates in the setting of Rotary ECAD (R-ECAD), resulting in a procedure recognized for its efficacy. The tool is firmly secured to a collet that is free to spin in this approach, and the connections are made in the same way as in the traditional ECAD configuration. The addition of rotating motion to the tool has proved to offer greater performance, significantly lowering concerns such as overcut, Heat Affected Zone (HAZ), taper, and overall machining time. The benefit of tool rotation is that it distributes sparks equally over the tool's perimeter. This equal dispersion of sparks leads to even and smooth machining, which helps to create smooth hole surfaces. Overcut was seen to reduce greatly up to 1500 rpm, but beyond that speed, overcut began to grow [38]. The turbulence induced in the electrolyte is responsible for the rise in overcut at greater rotation speeds. At high rotation speeds, the hot electrolyte tends to travel away from the machining zone, causing discharge processes to destabilize. This might cause stray sparking around the tool, worsening the overcut problem. Nonetheless, Rotary-ECAD has shown its promise by obtaining a high aspect ratio in the drilling of tiny holes in glass, enhancing circularity [39]. Furthermore, while drilling micro holes in Al_2O_3 ceramics, Rotary-ECAD has been effectively used to improve hole circularity and obtain a maximum MRR of 0.125 mg/min [40]. It's also been used to drill minute holes in difficult-to-cut steel materials. Micro holes have been successfully drilled in borosilicate glass piece by rotating the workpiece dipped inside the electrolyte at a rotational speed of 40-80 rpm. The tool was given the ultrasonic vibrations in vertical manner and the rotational motion was provided with the help of a micro-metal gear DC motor attached to the base of fixture that holds the workpiece [41].

With a focus on multi-objective factors including MRR and Hole overcut (HOC), this study investigates the effects of various input variables on the Rotary-Electrochemical Arc Drilling (R-ECAD) process. The performance study of the R-ECAD process with regard to these multi-objective variables has received relatively little attention, in contrast to the current research, which focuses primarily on the effect of input variables on response variables in the ECAD process. In addition, there appears to be a lack in the research discussing the use of Grey Relational Analysis (GRA) for multi-objective optimisation in the R-ECAD process, with the goal of simultaneously maximising MRR and minimising HOC. The new assessment of input variables, such as like tool feed rate, work material rotational speed and applied voltage, in the context of micro-hole production on glass material utilising R-ECAD is investigated in this research in order to fill in these gaps. The goal of the study, which uses GRA to accomplish multi-objective optimisation, is to determine the best sets of input variable combinations for improved process performance.

2. MATERIALS AND METHODS

By developing and manufacturing the rotary assisted electrochemical discharge-based drilling process (R-ECAD) equipment, as illustrated in Figure 2, an entirely new technique of micro-hole drilling is provided. A HY3040 CNC machine and computer-controlled software are included in the setup. It also considers the rotational speed application of the working material during the ECAD process. The fixture that the glass material is fixed to rotates with the help of an MMG DC motor with a range of 0-100 rpm. The seepage motion that results from the work material rotating produces the spark that is produced during the process and adds stability to the hydrogen gas film creation. The DC power supply provides voltage to the tool and auxiliary anode. The CNC programme controls the tool feed rate as well as the movements of the X and Y axes. Viewers can see the configuration and components utilised in this complex machining process in Figure 2. The comparison of the micro-holes drilled with and without R-ECAD process is shown through microscopy images in Figure 3.

2.1. Measurements

Following the creation of micro-holes, measurements of the working material are carried out to perform the multi-objective optimization. Three measurements are averaged to reduce computational mistakes.

2.1.1. MRR

The difference in the weight of the soda lime glass working material before and after R-ECAD process in a unit of time is used to compute the MRR. The following is the offered MRR formula (1).

$$\text{MRR} = ((w_{h1} - w_{h2})/t)) \quad (1)$$

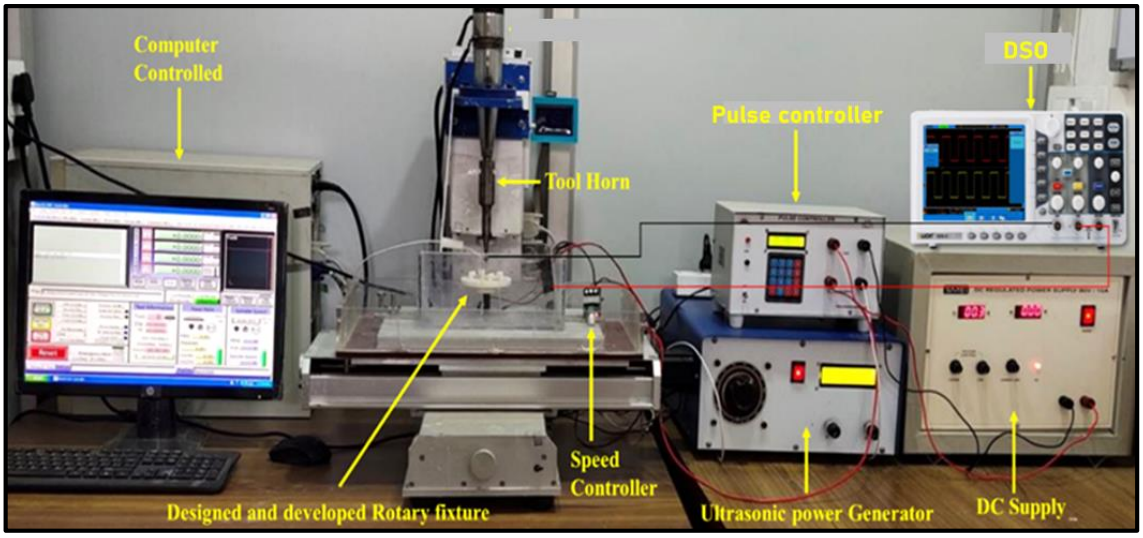

Fig. 2. Designed Experimental setup of R-ECAD process

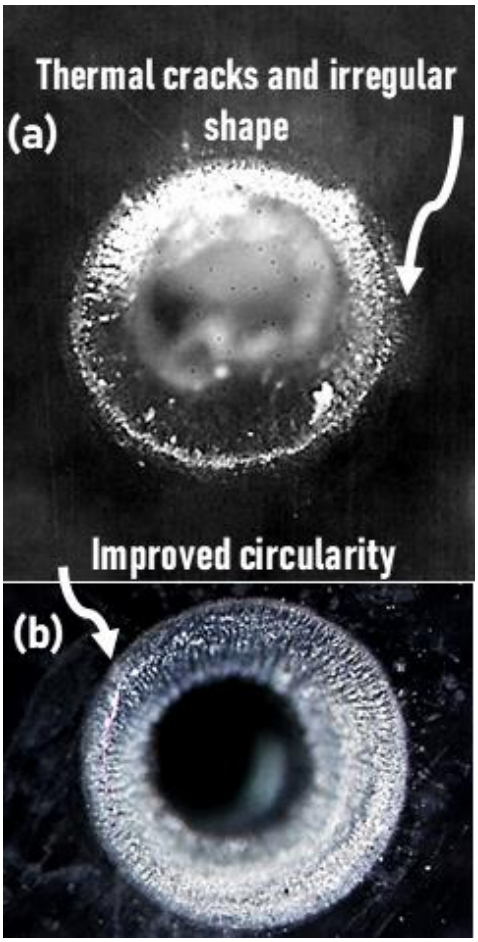

Fig. 3. Microscopy images of the micro-holes drilled at initial input factors (a) ECAD Process (b) R-ECAD process.

where w_{h1} = weight before R-ECAD process and w_{h2} = weight after R-ECAD process.

2.1.2. HOC

The difference between the tool diameter (d) and the measured diameter of the hole entry (D_{ent}) is known as hole overcut. Figure 4 depicts an example of HOC during the ECAD process.

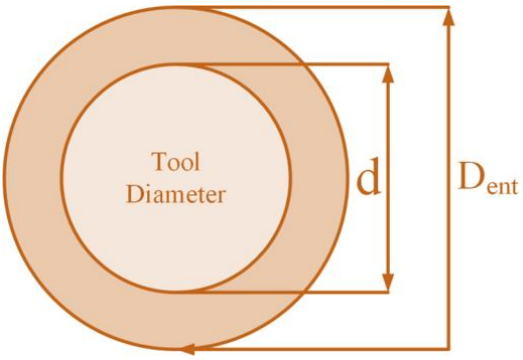

Fig. 4. Schematic diagram for HOC measurement

3. RESULTS AND DISCUSSION

3.1. Signal to Noise ratio analysis:

As indicated in Table 2, S/N analysis includes assessing the individual parametric combinations of input variables for all measured responses. S/N ratios are determined as follows for responses with a "higher-the-better" aim, such as MRR:

Table 1. Input Variables and their levels utilized during ECAD optimization study

Input Variables					**Fixed Variables**	
Levels	**Units**	**I**	**II**	**III**	Primary tool	Tungsten Carbide
A: Working material rotation (WR)	rpm	50	60	70	Electrolyte	KOH
B: Tool Feed Rate (FR)	mm/min	0.6	0.7	0.8	Secondary tool	Graphite
C: Applied Voltage (AV)	V	35	40	45	Drilling time	2 minutes

Table 2. Measured responses and corresponding S/N ratios in ECAD process

Exp.	**WR (rpm)**	**FR (mm/min)**	**AV (V)**	**MRR (mm^3 /min)**	**HOC (mm)**	**S/N ratio (MRR)**	**S/N ratio (HOC)**
1	50	0.6	35	0.9582	0.2385	-0.370877	12.4502
2	50	0.7	40	0.9485	0.2298	-0.459253	12.7730
3	50	0.8	45	0.9324	0.2365	-0.607955	12.5234
4	60	0.6	40	0.9723	0.2158	-0.243994	13.3190
5	60	0.7	45	0.9642	0.2043	-0.316657	13.7946
6	60	0.8	35	0.9512	0.2015	-0.434563	13.9145
7	70	0.6	45	0.9748	0.2397	-0.221690	12.4066
8	70	0.7	35	0.9415	0.2049	-0.523594	13.7692
9	70	0.8	40	0.9274	0.1987	-0.654658	14.0360

$$S/N = -10\log_{10}[\frac{1}{n}\sum_{i=1}^{n}\left(\frac{1}{MRR_i}\right)^2] \quad (3)$$

On the other hand, when calculating the S/N ratio for responses with a "smaller-the-better" such as HOC, the expression is as follows:

$$S/N = -10\log_{10}[\frac{1}{n}\sum_{i=1}^{n}(HOC_i)^2 \quad (4)$$

In this case, 'n' represents the number of measurements, and 'i' represents the reaction.

A larger S/N ratio magnitude is often seen as indicating the most relevant variable in getting desired results. The mean of the S/N ratio and the delta value are used in this study to determine the best combination of input factors. The delta value is calculated as the difference between the response's lowest and highest mean values.

3.1.1. Analysis of input factors impacting MRR

The primary effect of input factors on MRR is shown in Figure 5, it depicts the link between the S/N ratio and MRR. In addition, Table 3 offers delta values for the MRR response, which correspond to the findings as shown in Figure 5. These delta values represent the differences between the lowest and highest mean MRR values, offering information on how MRR varies under different experimental situations. The delta value demonstrates that Tool feed rate (FR) has the greatest effect on MRR (Rank 1, 0.2869) followed by the working material rotation (Rank 2, 0.1476) and lastly by applied voltage (Rank 3, 0.0705). Figure 6 adds to this information by displaying a scatter plot of the connection between MRR and the input factors. The ideal input factor configuration for maximizing the MRR is BIAIICIII, which corresponds to the values (0.6 mm/min, 60 rpm, 45 V). Taking into account the interactions of FR, WR & AV, this combination reflects the most favourable factors for obtaining the required MRR result of maximum value.

Table 3. S/N ratio mean for MRR

S/N Ratio Mean of MRR			
Level	**WR (rpm)**	**FR (mm/min)**	**AV (V)**
1	-0.4794	-0.2789	-0.4430
2	-0.3317	-0.4332	-0.4526
3	-0.4666	-0.5657	-0.3821
Delta	0.1476	0.2869	0.0705
Rank	**2**	**1**	**3**

The results demonstrate that as the rotating speed of the work material increases, so does the MRR. This is due to the better drilling of micro holes made possible by the rotating motion [56], which results in greater machining depth. Additionally, greater rotational speed adds to improved electrolyte circulation between the tool and the working material. This method has a significant benefit in that the energy from the spark is equally spread over the whole drilling region, resulting in straight and precisely cut holes. An improvement of 0.0141 mm^3/min in MRR is noticed with the increase of WR from 50 rpm to 60 rpm (Figures 5& 6, Exp. 1 & 4). Figure 7 shows the corresponding microscopy images of the micro-holes drilled using R-ECAD. It is worth noting, however, that at extremely high WR, the MRR tends to decrease. This is mostly due to electrolyte splashing, which hinders the formation of the gas layer, as depicted in Figures 5 & 6(a). The tool feed rate plays a critical role in MRR, as shown in Figure 6 (a & c) and explained in Table 3. Notably, increasing the tool feed rate leads to a drop in MRR.

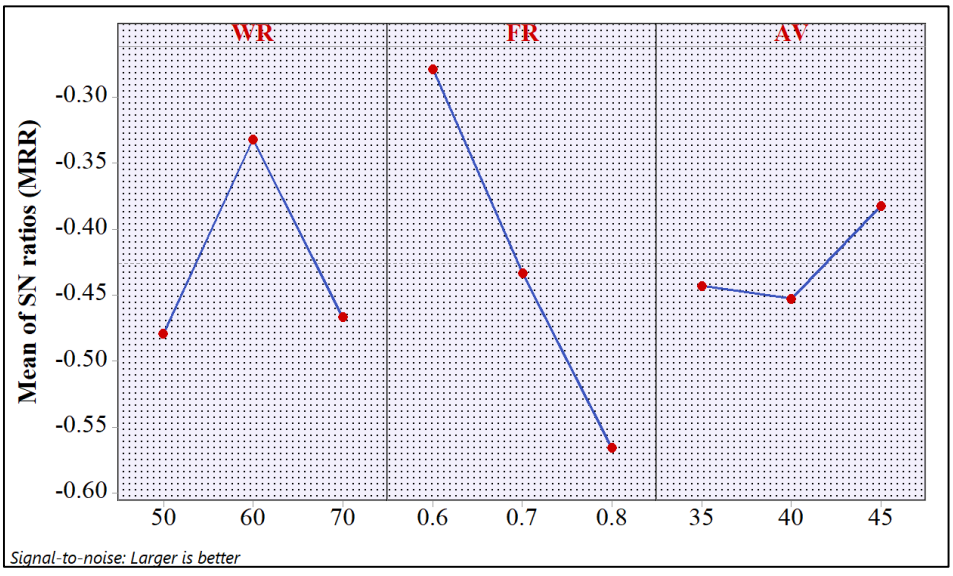

Fig. 5. Mean graph of MRR vs WR, FR & AV

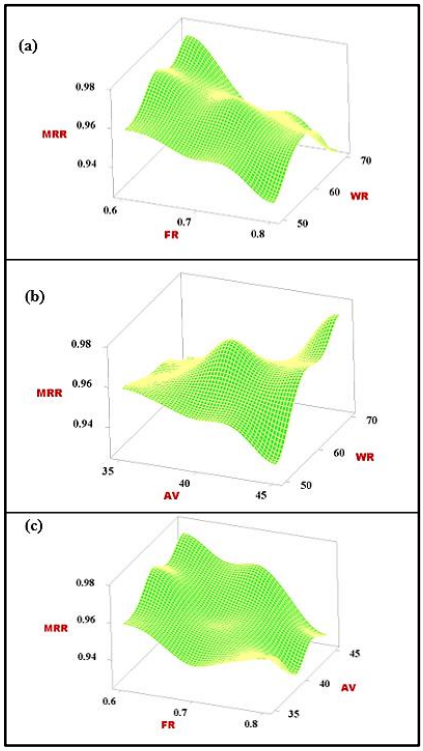

Fig. 6. Surface plot of MRR with respect to (a) WR & FR (b) WR & AV (c) FR & AV

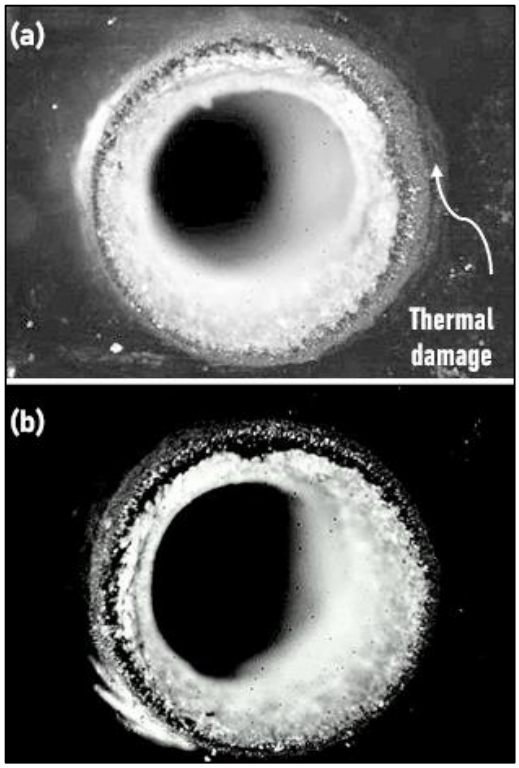

Fig. 7. Microscopy images of drilled micro-holes (a) 50 rpm, 0.6 mm/min, 35 V (b) 60 rpm, 0.6 mm/min, 40 V

This phenomenon may be explained by the fact that greater tool feed rates result in fewer contacts between the tool and the work material, resulting in a decrease in heat energy inside the drilling region. In essence, the decreased MRR found at higher FR, is a result of this diminished contact, emphasising the delicate balance necessary to optimise the machining process and achieve desirable MRR. Further, MRR increases noticeably with increasing applied voltage, as seen in Figure 5 & 6 (b-c).

This enhancement can be due to higher voltage levels causing more hydrogen bubbles to develop at the tool-electrolyte interface. This, in turn, increases the formation of a gas layer, resulting in high-intensity sparks, especially over the soda lime glass material. As a result, high MRR is obtained.

3.1.1. Analysis of input factors impacting HOC

The primary effect of input factors on HOC is shown in Figure 6, it depicts the link between the S/N ratio and HOC. In addition, Table 4 provides the delta values for the HOC response, which is similar to the findings as shown in Figure 8. The delta value demonstrates that working material rotation has the greatest effect on MRR (Rank 1, 1.09) followed by the tool feed rate (Rank 2, 0.77) and lastly by applied voltage (Rank 3, 0.47). Figure 9 shows this information by displaying a scatter plot of the connection between HOC and the input factors. The ideal input factor configuration for minimising HOC is AIIBIIICI, which corresponds to the values (60 rpm, 0.8 mm/min, 35 V). Taking into account the interactions of FR, WR & AV, this combination reflects the most favourable factors for obtaining the minimum HOC. It is observed that HOC improves with the increase in working rotation upto first level then it again deteriorates with the change in level from 60 rpm to 70 rpm.

Table 4. S/N ratio mean for HOC

S/N Ratio Mean of HOC			
Level	**WR (rpm)**	**FR (mm/min)**	**AV (V)**
1	12.58	12.73	13.38
2	13.68	13.45	13.38
3	13.40	13.49	12.91
Delta	1.09	0.77	0.47
Rank	**1**	**2**	**3**

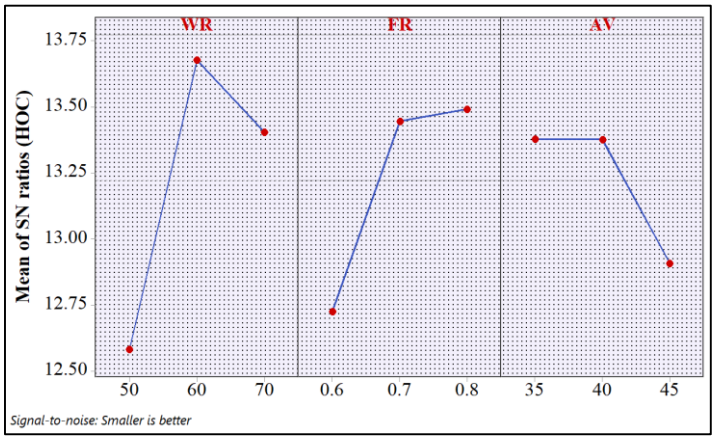

Fig. 8. Mean graph of HOC vs WR, FR & AV

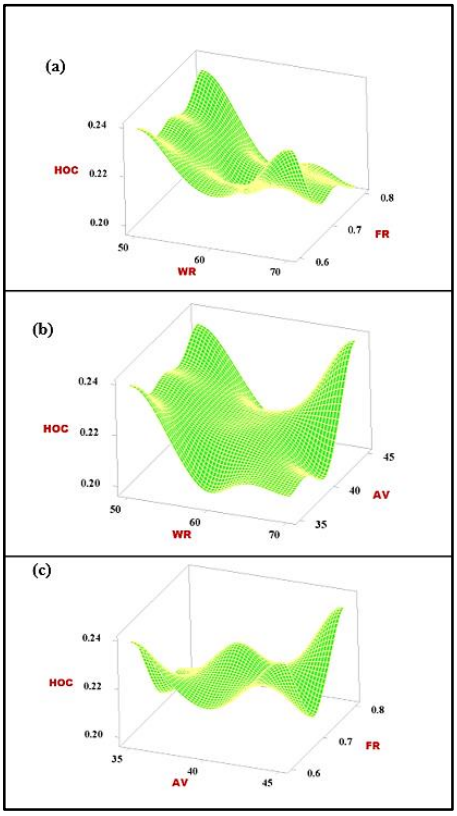

Fig. 9. Figure 4 Surface plot of HOC with respect to (a) WR & FR (b) WR & AV (c) FR & AV

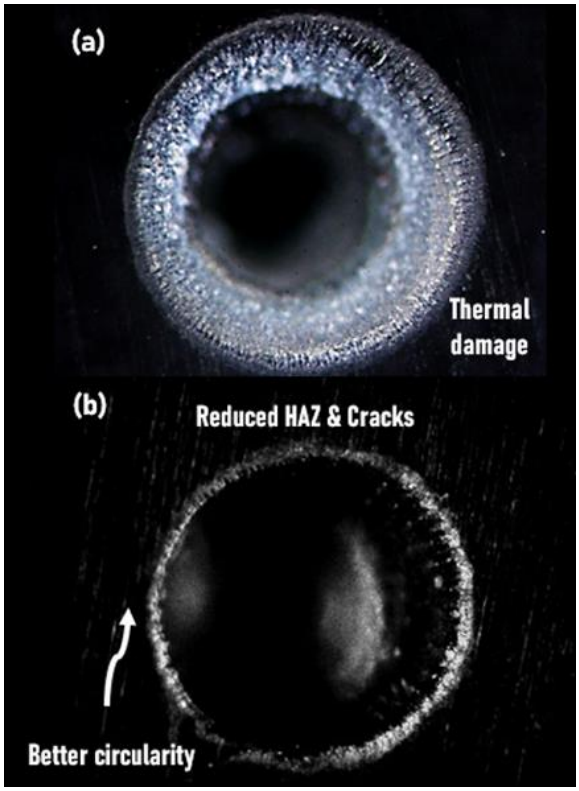

Fig. 10. Microscopy images of drilled micro-holes (a) 50 rpm, 0.7 mm/min, 40 V (b) 60 rpm, 0.8 mm/min, 35 V

Any improvement in the HOC due to the assistance of the rotation is noticeable due to the enhancement in the availability of the electrolyte and uniform distribution of the thermal energy in the drilling region. An improvement of 0.0227 mm in HOC is noticed with the increase of WR from 50 rpm to 60 rpm (Figures 7-9, Exp. 1 & 4). As a whole, an enhancement in HOC is obtained. With the further increase in the working material rotation, the gas layer tends to become unstable due to electrolyte splashing because of centrifugal forces. Thus, a decrease in the improvement of the HOC.

At greater FR, HOC tends to decrease because to decreasing contact between the tool and the working material. As a result, less heat energy is transmitted in the drilling region. HOC improves when FR escalates, as expected, because heat energy transfer via sparks diminishes. Figure 10 shows the microscopy images of the micro-holes produced using R-ECAD process at two different experimental conditions. The geometrical characteristics of the micro-holes are clearly improved with the increase of WR and increase of FR as visible from the figure 10 (Experiment no. 2 & 6). The cracks produced during the micro-hole's fabrication has also decreased with the increase in WR rotational effect in R-ECAD process. The effect of applied voltage is observed similar as discussed in the case of MRR, that is high intensity of sparks are generated with the level increase of voltage from 35 V to

45V and from 45 V to 50 V respectively. More number of sparks in the drilling region tends to increase the HOC. Thus, HOC improves at lower level of applied voltage because of reduced thermal damage.

3.2. Multi-objective response optimization

Response factors including MRR and HOC demonstrate sensitivity to any changes in input factors. The S/N Ratio analysis shows that the highest MRR is obtained at a high level of working material rotation, applied voltage and low level of tool feed rate voltage (BIAIICIII). On the other hand, the optimum value of input factors for HOC are calculated as AIIBIIICI (Table 3 & 4).

Finding the optimal combination of techniques for multi-objective optimization is a real challenge. To solve this problem, the multi-objective optimization method of Gray Relational Analysis (GRA) is used to determine the optimal combination.

3.2.1. Grey relational analysis (GRA)

The optimisation of multi-objective response factors in the context of Grey Relational Analysis (GRA) entails changing it into a single-objective optimisation issue. The GRA procedure is divided into three steps: (i) Grey Relational Generation, (ii) Grey Relational Coefficients (GRC), and (iii) Grey Relational Grades (GRDs). The experimental findings of all response factors are normalised using Equations 5 and 6, respectively, during the Grey Relational Generation phase. This normalisation is required to achieve a similar sequence in the 0-1 range [42-43]. The measured answers are divided into two groups: "higher-the-better" and "smaller-the-better." Equation 5 is used to normalize responses that fall into the "higher-the-better" category, such as MRR while Equation 6 is used for responses that fall into the "smaller-the-better" category, such as HOC. These normalisation stages are critical for assuring consistency and comparability of response factors.

$$y_i = \frac{\max(x_i) - (x_i)}{max(x_i) - \min(x_i)} \tag{5}$$

$$y_i = \frac{(x_i) - \min(x_i)}{max(x_i) - \min(x_i)} \tag{6}$$

Table 5. GRA components calculated for response factors: GRGs, GRCs and Normalized values.

Exp.	Normalized value		GRC		GRG (Grey Relational Grades)	
	MRR	HOC	MRR	HOC	Value	Order
1	0.7561	0.0293	0.6721	0.3400	0.5060	5
2	0.5882	0.2415	0.5484	0.3973	0.4728	6
3	0.3097	0.0780	0.4201	0.3516	0.3858	9
4	1.0000	0.5829	1.0000	0.5452	0.7726	2
5	0.8599	0.8634	0.7811	0.7854	0.7833	1
6	0.6349	0.9317	0.5780	0.8798	0.7289	3
7	0.3616	0.0000	0.4392	0.3333	0.3863	8
8	0.1730	0.6049	0.3768	0.5586	0.4677	7
9	0.0000	1.0000	0.3333	1.0000	0.6667	4

In the provided equations, y_i represents the normalized value, y_i is the measured response value, 'min' and 'max' denote the minimum and maximum values of x_i and *i* signifies the number of response sequences. The next step includes utilising Equation 7 to calculate the GRC once the sequence has been normalised. The identification coefficient, denoted by the factor " in this equation, has a value that might be between 0 and 1. Each factor is given equal weight in this study, hence is set to 0.5, a standard value in GRA. The normalised values and associated GRCs for the response factors are provided in the table.

$$\text{GRC} = \epsilon_i(k) = \frac{\Delta_{min} + \beta\Delta_{max}}{\Delta_i + \beta\Delta_{max}} \tag{7}$$

Where, Δ_i is the difference between the maximum and sequential response factors, $\Delta_{min}\ and\ \Delta_{max}$ is the minimum and maximum value of Δ_i.

Grey Relational Grades (GRG) is obtained by considering average of GRC values as given in Eq. 8.

$$GRG = (\gamma i) = \frac{1}{n}\sum_{k=1}^{n} €_i(k) \quad (8)$$

Table 5 shows the relationship between the estimated GRGs for all the input factors' combination while Table 6 presents the mean of GRG along with their corresponding ranks. According to a higher-order GRG, the results of the experiment for that grade are more likely to meet the optimum response requirements [52]. As a result, the GRG analysis determined that the AIIBICII (60 rpm, 0.7 mm/min, 45 V) combination of optimal factors for this investigation corresponds to experiment 5.

However, taking into account all three levels is crucial in order to fully comprehend the influence of each control factor on the grey relational grades. Thus, as shown in Figure 11, the final combination of input process factors is determined using the GRG means.

The best combination for the combined response factors—high MRR and low HOC is found to be AIICIIBIII (60 rpm, 40 V, 0.8 mm/min) using the delta ranking technique. The results show that the rotational effect has the maximum influence on the multi-objective responses followed by the applied voltage and feed rate of the tool. Medium level of work material rotation results into the stable formation of the gas layer and as a result, better spark uniformity around the tool is observed. The medium level of applied voltage is necessary to acquire the high MRR and low HOC since high level of applied voltage tends to result in higher HOC due to increase in spark intensity over the soda lime glass material. As a result, medium applied voltage results in favorable HOC and MRR results. The influence of the thermal energy due to spark decrease in the drilling region at a high tool feed rate because of reduced interaction between the tool and soda lime glass. Thus, lower level of tool feed rate is favorable for reducing low HOC and preferrable MRR.

3.2.2. Confirmation tests

For the purpose of confirming the enhancement of the response factors at the optimal level, confirmation tests must be carried out. Eq. 9 is used to forecast the GRG.

$$\bar{\gamma} = \gamma m + \sum_{i=1}^{k} (\bar{\gamma} i - \gamma m) \quad (9)$$

where, γ_m is the total mean GRG, , $\bar{\gamma}_k$ is the mean GRG at the optimum level of factors, $\bar{\gamma}$ is the predicted GRG, and k is the number of input factors. Total mean GRG is 0.5745.

The computed GRG was determined to be 0.8864 at the optimal levels of the input process factors (AII, BIII, and CII). Table 7 displays the results of the confirmation test carried out at these optimal values. The findings of the confirmation tests, which were calculated as the average of three trials, closely match the outcomes that were expected based on the grey relational grades.

Notably, the GRG has improved noticeably by 39% between the ideal settings (AIIBIIICII) and the beginning condition (AIIBIICII).

Table 6. GRG mean and corresponding ranks

Mean GRG			
Level	**WR**	**FR**	**AV**
1	0.4549	0.5550	0.5675
2	0.7616	0.5746	0.6374
3	0.5069	0.5938	0.5185
Delta	0.3067	0.0388	0.1189
Rank	**1**	**3**	**2**

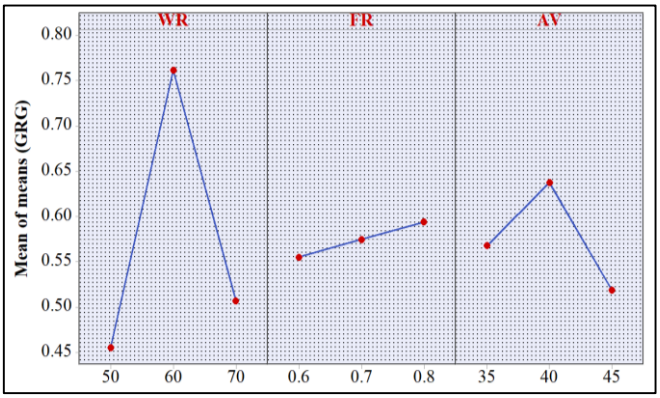

Fig. 11. Mean graph of GRG

Table 7. Confirmation results of GRG

Level of input factors		GRG of response factors
Initial input factors (AI, BII, CIII)		0.6414
Optimum levels of input factors (AII, BIII, CII)	Predicted	0.8438
	Experimental	0.8970

Figure 12 shows the microscopic images of the micro-holes drilled at initial input factors and optimum input factors. A significant improvement in the HOC and geometrical features in terms of heat affected zone and thermal cracks are observed when holes are drilled at optimum input factors.

4. CONCLUSIONS

This investigation is focused on multi-objective optimization of the R-ECAD input factors for maximizing the MRR and minimizing the HOC during the micro-drilling of soda lime glass material in order to conduct a thorough performance evaluation.
The S/N ratio and GRA are used to systematically analyses the machining performance and determine the ideal range of input factors. By reducing the multi-objective optimisation to a more manageable single-objective optimisation, the benefit of using GRA over the S/N ratio is highlighted. The following is a summary of the main findings of this investigation:

- S/N ratio reveals that for maximizing the MRR, the optimum input factor combination is BIAIICIII (0.6 mm/min, 60 rpm, 45 V) while for minimizing the HOC, the combination is AIIBIIICI (60 rpm, 0.8 mm/min, 35 V).
- Working material rotational effect enhances the MRR as well as HOC because of better replenishment of the electrolyte in the drilling region. It produces thin gas layer and better spark uniformity.
- GRA based optimized input factors obtained for multi-objective criteria in R-ECAD is AIICIIBIII (60 rpm, 40 V, 0.8 mm/min).
- The work material rotational effect is the most influential input factors followed by the applied voltage and tool feed rate. Applied voltage is the second most determinant in the combination since it directly controls the amount of heat energy in the drilled region of R-ECAD process.
- An improvement of 39 % in the GRG is noticed when responses are measured at the optimum combination of the input factors in contrast to initial machining input factors.
- This methodology proves to be well-suited for performing the multi-objective response optimization and can be effectively used to obtain the optimum combination of the input factors for enhancing the performance of rotary assisted electrochemical arc drilling (R-ECAD) process.

Acknowledgement
Authors acknowledge the support given by the Punjab Engineering college, Chandigarh, India.

Conflicts of Interest: There is no conflict of interest.

REFERENCES

1. Mehrabi, F., Farahnakian, M., Elhami, S., Razfar, M. R. (2018). *Application of electrolyte injection to the electro-chemical discharge machining (ECDM) on the optical glass*. Journal of Materials Processing Technology, 255, 665-672. https://doi.org/10.1016/j.jmatprotec.2018.01.016
2. Singh, T., Dvivedi, A. (2016). *Developments in electrochemical discharge machining: A review on electrochemical discharge machining, process variants and their hybrid methods*. International journal of machine tools and manufacture, 105, 1-13. https://doi.org/10.1016/j.ijmachtools.2016.03.004
3. Arya, R. K., Dvivedi, A. (2023). *Improving the electrochemical discharge machining (ECDM) process for deep-micro-hole drilling on glass by application of the electrolyte-air injection*. Ceramics International, 49(6), 8916-8935. https://doi.org/10.1016/j.ceramint.2022.11.047
4. Rajput, V., Goud, M., Suri, N. M. (2019). *Study on effective process parameters: toward the better comprehension of ECDM process*. Int J Mod Manuf Tech, 11, 105-118.
5. Rajput, V., Goud, M., Suri, N. M. (2021). *Multi-spark simulation of the electrochemical discharge machining*

(ECDM) process. Journal of Mechanical Science and Technology, 35, 5127-5135. https://doi.org/10.1007/s12206-021-1029-7
6. Ho, C. C., Chen, J. C. (2020). *Micro-drilling of sapphire using electro chemical discharge machining*. Micromachines, 11(4), 377. https://doi.org/10.3390/mi11040377
7. Arya, R. K., Paliwal, S., Dvivedi, A., Maran, R. (2022). *Investigation on deposition of the machined by-products and its reduction during electrochemical discharge machining (ECDM)*. Journal of The Electrochemical Society, 169(2), 023506. DOI 10.1149/1945-7111/ac4f6f
8. Bajpai, V. K., Mishra, D. K., Dixit, P. (2022). *Fabrication of Through-glass Vias (TGV) based 3D microstructures in glass substrate by a lithography-free process for MEMS applications*. Applied Surface Science, 584, 152494. https://doi.org/10.1016/j.apsusc.2022.152494
9. Ben Said, L., Kolsi, L., Ghachem, K., Almeshaal, M., Maatki, C. (2023). *Application of nanofluids as cutting fluids in machining operations: A brief review. Applied Nanoscience*, 13(6), 4247-4278. https://doi.org/10.1007/s13204-021-02140-8
10. Torabi, A., & Razfar, M. R. (2021). *The capability of ECDM in creating effective microchannel on the PDMS*. Precision Engineering, 68, 10-19. https://doi.org/10.1016/j.precisioneng.2020.11.004
11. Singh T, Arab J, Dixit P. (2022), *A review on microholes formation in glass-based substrates by electrochemical discharge drilling for MEMS applications*. Machining Science and Technology., 4, 26(2), 276-337. https://doi.org/10.1080/10910344.2022.2044857
12. Grover, S., MANGAL, S., Singh, S., SINGH, M., Rajput, V., Sharma, S., Abbas, M. (2024). *Experimental investigation for micro-machining of borosilicate glass using ultrasonic assisted rotary electrochemical discharge machining (UA-RECDM) process*. Journal of Micromechanics and Microengineering. DOI 10.1088/1361-6439/ad3658
13. Kumar, A., Goud, M., Kant, S., Rajput, V. (2024). *Synergistic modeling for precision in electrochemical discharge mechanism: a triad of 3D finite element, ANN, and regression approaches*. Multiscale and Multidisciplinary Modeling, Experiments and Design, 1-16. https://doi.org/10.1007/s41939-024-00449-9
14. Rajput, V., Goud, M., Suri, N. M. (2020). *Performance analysis of ECDM process using surfactant mixed electrolyte*. In Manufacturing Engineering: Select Proceedings of CPIE 2019 (pp. 285-300). Springer Singapore. https://doi.org/10.1007/978-981-15-4619-8_22
15. Sabahi, N., Razfar, M. R., Hajian, M. (2017). *Experimental investigation of surfactant-mixed electrolyte into electrochemical discharge machining (ECDM) process*. Journal of Materials Processing Technology, 250, 190-202. https://doi.org/10.1016/j.jmatprotec.2017.07.017
16. Rajput, V., Goud, M., Suri, N. M. (2020). *Finite element modeling based material removal analysis of non-conductive materials in ECDM using adaptive tool feed system*. International Journal of Modern Manufacturing Technology, 12(1), 164-173.
17. Huang, S. F., Liu, Y., Li, J., Hu, H. X., & Sun, L. Y. (2014). *Electrochemical discharge machining micro-hole in stainless steel with tool electrode high-speed rotating*. Materials and Manufacturing Processes, 29(5), 634-637. https://doi.org/10.1080/10426914.2014.901523
18. Jiang, B., Lan, S., Ni, J., Zhang, Z. (2014). *Experimental investigation of spark generation in electrochemical discharge machining of non-conducting materials*. Journal of Materials Processing Technology, 214(4), 892-898. https://doi.org/10.1016/j.jmatprotec.2013.12.005
19. Jiang, B., Lan, S., Ni, J. (2015, June). *On modeling and simulation of the discharging activity in electrochemical discharge machining*. In International Manufacturing Science and Engineering Conference (Vol. 56826, p. V001T02A050). American Society of Mechanical Engineers. https://doi.org/10.1115/MSEC2015-9456
20. Sharma, S., Singh, T., Dvivedi, A. (2023). *A review on developments in electrolytes and their feeding methods for ECDM process*. Silicon, 15(4), 1571-1595. https://doi.org/10.1007/s12633-022-02134-3
21. Rajput, V., Goud, M., Suri, N. M. (2023). *Enhancement of Electrochemical Discharge Machining (ECDM) Characteristics with Tool Electrode Rotation*. In Advances in Modelling and Optimization of Manufacturing and Industrial Systems: Select Proceedings of CIMS 2021 (pp. 135-148). Singapore: Springer Nature Singapore. https://doi.org/10.1007/978-981-19-6107-6_11
22. Rajput, V., Bhinder, J., Singh, G. (2023). *Research Progress of Self-Healing Elastomers Materials: Processing and Characterization*. Materials for Biomedical Simulation: Design, Development and Characterization, 59-69. https://doi.org/10.1007/978-981-99-5064-5_3
23. Rajput, V., Goud, M. M., Suri, N. M. (2019). *Performance Analysis on the Effect of Different Electrolytes during Glass Micro Drilling Operation Using ECDM*. I-manager's Journal on Future Engineering and Technology, 14(4), 5–13.
24. Grover, S., Singh, S., Mangal, S. K. (2023). *Hybridization of μ-electrochemical discharge machining (μ-ECDM) process: A review*. Materials Today: Proceedings, 80, 499-508. https://doi.org/10.1016/j.matpr.2022.10.204
25. Grover, S., Singh, S., Mangal, S. K. (2023). *Hybridization of μ-electrochemical discharge machining (μ-ECDM) process: A review*. Materials Today: Proceedings, 80, 499-508.

https://doi.org/10.1016/j.matpr.2022.10.204
26. Rajput, V., Goud, M., Suri, N. M. (2022). *Performance analysis of closed-loop electrochemical discharge machining (CLECDM) during micro-drilling and response surface methodology based multi-response parametric optimisation*. Advances in materials and processing technologies, 8(2), 1352-1382. https://doi.org/10.1080/2374068X.2020.1860494
27. Rajput, V., Goud, M., Suri, N. M. (2021). *Review on recent advances, research trends, and gas film in electrochemical discharge-based micromachining*. Journal of Micro-and Nano-Manufacturing, 9(1), 010801. https://doi.org/10.1115/1.4049418
28. Rajput, V., Goud, M., Suri, N. M. (2021). *Electrochemical discharge machining: gas film electrochemical aspects, stability parameters, and research work*. Journal of the electrochemical society, 168(1), 013503. DOI 10.1149/1945-7111/abd516
29. Nawaz, S. A., Cao, P., Tong, H., Li, Y. (2023). *Micro ECDM scanning process with feedback control of flexible contact force*. Journal of Manufacturing Processes, 94, 266-277. https://doi.org/10.1016/j.jmapro.2023.03.058
30. Bhargav, K. V. J., Balaji, P. S., Sahu, R. K., Katiyar, J. K. (2023). *Exemplary approach using tool rotation-assisted μ-ECDM for CFRP composites machining*. Materials and Manufacturing Processes, 38(3), 271-283. https://doi.org/10.1080/10426914.2022.2072879
31. Gehlot, D., Jha, P. K., & Jain, P. K. (2024). *Experimental Investigation and Modelling Studies on MHD Convection in Magnetic-assisted-ECDM*. Materials and Manufacturing Processes, 39(4), 494-505. https://doi.org/10.1080/10426914.2023.2236207
32. Pawariya, K., Dvivedi, A., Singh, T. (2019). *On performance enhancement of electrochemical discharge trepanning (ECDT) process by sonication of tool electrode*. Precision Engineering, 56, 8-19. https://doi.org/10.1016/j.precisioneng.2018.08.016
33. Cheng, C. P., Wu, K. L., Mai, C. C., Yang, C. K., Hsu, Y. S., Yan, B. H. (2010). *Study of gas film quality in electrochemical discharge machining*. International Journal of Machine Tools and Manufacture, 50(8), 689-697. https://doi.org/10.1016/j.ijmachtools.2010.04.012
34. Singh, T., Dvivedi, A. (2022). *Impact of gas film thickness on the performance of RM-ECDM process during machining of glass*. Materials and Manufacturing Processes, 37(6), 652-663. https://doi.org/10.1080/10426914.2021.1945092
35. Kolhekar, K. R., Sundaram, M. (2018). *Study of gas film characterization and its effect in electrochemical discharge machining*. Precision Engineering, 53, 203-211. https://doi.org/10.1016/j.precisioneng.2018.04.002
36. Harugade, M. L., Kavade, M. V., Hargude, N. V. (2013). *Effect of electrolyte solution on material removal rate in electrochemical discharge machining. IOSR* Journal of Mechanical and Civil Engineering (IOSR-JMCE), 5, 1-8.
37. Gupta, P. K., Dvivedi, A., Kumar, P. (2014). *A study on the phenomenon of hole overcut with working gap in ECDM*. J. Prod. Eng., 17(November), 1-5.
38. Zheng, Z. P., Su, H. C., Huang, F. Y., Yan, B. H. (2007). *The tool geometrical shape and pulse-off time of pulse voltage effects in a Pyrex glass electrochemical discharge microdrilling process*. Journal of Micromechanics and Microengineering, 17(2), 265. DOI 10.1088/0960-1317/17/2/012
39. Jui, S. K., Kamaraj, A. B., Sundaram, M. M. (2013). *High aspect ratio micromachining of glass by electrochemical discharge machining (ECDM)*. Journal of Manufacturing Processes, 15(4), 460-466. https://doi.org/10.1016/j.jmapro.2013.05.006
40. Dhanvijay, M. R., Ahuja, B. B. (2021). *Experimental Investigation On Rotary ECDM Process Of Al_2 O_3 Ceramics*. Journal of Manufacturing Technology Research, 13(3/4), 201-213.
41. Coteață, M., Schulze, H. P., & Slătineanu, L. (2011). *Drilling of difficult-to-cut steel by electrochemical discharge machining.* Materials and Manufacturing Processes, 26(12), 1466-1472. https://doi.org/10.1080/10426914.2011.557286
42. Bellubbi, S., N, S., Mallick, B. (2022). *Multi response optimization of ECDM process parameters for machining of microchannel in silica glass using Taguchi–GRA technique*. Silicon, 14(8), 4249-4263. https://doi.org/10.1007/s12633-021-01167-4
43. Rajput, V., Pundir, S. S., Goud, M., Suri, N. M. (2021). *Multi-response optimization of ECDM parameters for silica (quartz) using grey relational analysis*. Silicon, 13, 1619-1640. https://doi.org/10.1007/s12633-020-00538-7

Received: October 14th, 2023 / Accepted: June 15th, 2024 / Paper available online: June 20, 2024